Journal of Process Control 23 (2013) 179–188

Contents lists available at SciVerse ScienceDirect

Journal of Process Control

journal homepage: www.elsevier.com/locate/jprocont

Data-driven, using design of dynamic experiments, versus model-driven optimization of batch crystallization processes

Andrew Fiordalis, Christos Georgakis*

Department of Chemical and Biological Engineering, Tufts University, Medford, MA 02155, USA

ARTICLE INFO

Article history:
Received 16 March 2012
Received in revised form 10 August 2012
Accepted 14 August 2012
Available online 10 October 2012

Keywords:
Optimization
Design of experiments
Batch crystallization
Batch processes
Data-driven modeling

ABSTRACT

A new data-driven experimental design methodology, design of dynamic experiments (DoDE), is proposed as a means of developing a response surface model that can be used to effectively optimize batch crystallization processes. This data-driven approach is especially useful for complex processes for which it is difficult or impossible to develop a knowledge-driven model in a timely fashion for the optimization of an industrial process. Design of dynamic experiments [1] generalizes the formulation of time-invariant design variables from design of experiments, allowing for consideration of time-variant design variables in the experimental design. When combined with response surface modeling and an appropriate optimization algorithm, a data-driven optimization methodology is produced, which we call DoDE optimization. The method is used here to determine the optimal cooling rate profile, which integrates to give the optimum temperature profile, for a batch crystallization process. To examine the effectiveness of the DoDE optimization method, the data-driven optimum temperature profile is compared to the optimum temperature profile obtained using a model-based optimization technique for the potassium nitrate–water batch crystallization model developed by Miller and Rawlings [2]. The temperature profiles calculated using DoDE optimization yield response values within a few percent of the true model-based optimum values. A sensitivity analysis is performed on one case study to evaluate the distribution of the response variable from each method in the presence of parameter and initial seed distribution variability. It is demonstrated that there is partial overlap in the distributions when only variability in the model parameters is evaluated and there is substantial overlap when variability is included in both the model and initial seed distribution parameters. From this evidence, it can be concluded that the DoDE optimization method has the potential to be a useful data-driven optimization tool for batch crystallization processes where a first-principles model is not available or cannot be developed due to time and/or cost constraints.

1. Introduction

Batch crystallization is an important unit operation commonly found in pharmaceutical and specialty/fine chemical industries where high-value products are produced in small batches. Process optimization is imperative for these high-value products in order to produce crystals with desirable properties, maximize yield, and minimize lot-to-lot variability. Current optimization methodologies typically require the use of a first-principles model. Model-based techniques work well, but models describing complex pharmaceutical crystallizations for systems exhibiting polymorphs, localized concentration and temperature gradients, or crystals with multiple internal coordinates do not generally exist. Data-driven techniques based on the design of experiment (DoE) methodology are useful for generating response surface models which can be used for process optimization, especially when the response variable cannot be modeled by a first-principles model. The major drawback of the DoE approach is its inability to systematically evaluate time-variant input profiles, such as temperature, antisolvent addition rate, or supersaturation, all of which are important in batch crystallization processes.

Simple, one-dimensional crystallization models that neglect crystal agglomeration and breakage are common in the literature [2,3] and provide insight into the mechanisms of the crystallization processes in terms of overall growth and nucleation kinetics. These models are often used in process optimization routines to determine an optimum trajectory (temperature, antisolvent, supersaturation) that will result in a desired crystal size distribution (CSD) [4,5] or an optimal objective function stated in terms of the moments of the CSD [2,6]. First-principle models for more complex crystallization systems (polymorphic crystallization systems, antisolvent systems with localized temperature and concentration

* Corresponding author. Tel.: +1 617 627 2573; fax: +1 617 627 3991.
E-mail address: christos.georgakis@tufts.edu (C. Georgakis).

0959-1524/$ – see front matter © 2012 Elsevier Ltd. All rights reserved.
http://dx.doi.org/10.1016/j.jprocont.2012.08.011

gradients, models predicting crystal agglomeration, breakage, filterability, purity, and/or stability), however, are more difficult to develop and are rarely found in the literature.

In many cases, the time and effort required to develop a comprehensive knowledge-driven crystallization model carries a high cost and the value added to the process through the development of such a model will not offset the cost. Furthermore, important optimization objectives such as purity, product stability, or downstream filterability are difficult to model from a first principles point of view. In such cases, optimizing a particular aspect of the final crystal size distribution via a first-principles model may not satisfy one of these more data-oriented optimization objectives.

The field has produced extensive research studies related to the optimum temperature profile for batch crystallizers [7,8]. In order to determine an optimum temperature trajectory, an objective function must be specified in terms of a desired characteristic of the CSD at the end of the batch. Examples of optimization objectives include maximizing seed growth, minimizing nucleation, achieving a desired target CSD, or maximizing or minimizing a characteristic of the final crystal distribution in terms of the moments of the CSD. Two techniques for treating the temperature profile in a model-based dynamic optimization problem include discretization [9,7] and parameterization [10]. There are few limitations on the shape of the temperature profile when it is discretized, however, when the temperature profile is parameterized the shape is limited by the parameterized function. Therefore, it is important to select a function that can produce a large number of profile shapes. In each case, determining the optimum temperature trajectory requires a first-principles crystallization model. The optimum temperature profile is found using a constrained, nonlinear optimization algorithm which maximizes or minimizes the objective function subject to the crystallization model and system constraints.

Optimum operating profiles have been determined for a number of different crystallization models using various objective functions. Optimum temperature profiles for batch cooling crystallizations have been determined for a citric acid-water system [10], a paracetamol-ethanol system [4], a potassium sulfate-water system [5,11], and a potassium nitrate-water system [2,6,9]. In each of these papers, the optimization is performed using relatively simple crystallization models. Each model consists of a one-dimensional population balance equation (PBE) coupled with a mass balance equation. Each model relies on similar assumptions: (1) size-independent growth; (2) no crystal agglomeration or breakage; (3) a nucleation rate equal to either the sum of the primary and secondary nucleation rates or based solely on the secondary nucleation rate; and (4) a perfectly mixed crystallizer with crystals homogeneously distributed and no temperature or concentration gradients. While these assumptions are valid in some cases, most crystallization processes are more complex, especially at the scale required in industry.

For more complex industrial crystallizations where the desired response cannot be directly modeled in a first-principles sense, DoE has successfully been applied. In one DoE study, a fractional factorial design was used to evaluate the effect of six operating variables on filtration resistance for a pharmaceutical crystallization [13]. The data collected were used to generate a first-order RSM without interaction terms, which was then used to calculate the optimal operating conditions that resulted in reduced filtration times for the process. This example shows the usefulness of DoE and RSM for process optimization when no first-principles model exists for the process. As stated earlier, the main drawback of DoE is its inability to evaluate time-varying input trajectories that usually arise when optimizing nonlinear batch processes.

This paper is a continuation of the work presented in [14]. We evaluate a new data-driven experimental design technique developed by Georgakis [1] called design of dynamic experiments (DoDE). Design of dynamic experiments is built upon the well-established design of experiments (DoE) [15] methodology and allows for the systematic evaluation of time-varying input trajectories in an experimental setting. When DoDE is combined with response surface modeling (RSM) [16] and linear/nonlinear optimization [17] a data-driven optimization technique is obtained, which we call *DoDE optimization*. The DoDE optimization methodology bypasses the need for a first-principles model and is beneficial for processes where a first-principles model does not exist or is too costly to develop or where the optimization objective cannot be modeled. In this work, we use the DoDE optimization approach to optimize the temperature trajectory for a batch crystallization and compare these results with those obtained using a model-based optimization technique. The current paper documents the DoDE approach using a published crystallization model [2] and finds that the DoDE optimum is comparable to the model-based optimum. This builds support for the DoDE optimization methodology and its ability to achieve an optimization result for crystallization processes without requiring a knowledge-driven model.

2. Crystallization model

The seeded, potassium nitrate–water batch crystallization model developed by Miller and Rawlings [2] was used to compare the DoDE optimization methodology to a well-established model-based optimization technique [18]. The model was solved in terms of the moments (μ_i, $i = 0, 1, 2, \ldots$) of the CSD using the method of moments developed by Hulburt and Katz [19]. Ward et al. [9] evaluated many crystallization objectives expressed in terms of the moments of the CSD and grouped the objective functions into two classes. The first class yielded optimal temperature profiles that resulted in early crystal growth (elevated supersaturation levels at the beginning of the batch), and the second yielded optimal temperature profiles that resulted in crystal growth later in the crystallization (elevated supersaturation levels towards the end of the batch). Based on these findings, two crystallization objectives were chosen to compare the DoDE and model-based optimum temperature profiles.

The first objective, denoted by m_0, aims at minimizing the ratio of the number of crystals at the end of the batch to the initial number of crystals. Consequently, it aims at minimizing secondary nucleation. It results in an early growth profile and is expressed in terms of the 0th moment of the CSD.

$$m_0 = \frac{\mu_{0,T}(t = t_b)}{\mu_{0,T}(t = 0)} \tag{1}$$

The second objective, denoted by m_3, aims at maximizing the volume (mass) of the crystals grown from seed to the volume (mass) of the crystals formed through secondary nucleation. It results in a late growth profile and is expressed in terms of the third moment of the CSD.

$$m_3 = \frac{\mu_{3,S}(t = t_b)}{\mu_{3,N}(t = t_b)} \tag{2}$$

In (1) and (2), T, S, and N represent the total moments of the CSD, the moments tracking the growth of the seed crystal distribution, and the moments representing the distribution of nucleated crystals, respectively. Here, t is the time and t_b is the batch time.

The total moments, seed moments, and nucleated crystal moments are related by, $\mu_{i,T} = \mu_{i,S} + \mu_{i,N}$, and the moments are defined in terms of their respective CSD's as

$$\mu_{i,j}(t) = \int_0^\infty x^i n_j(x,t)\mathrm{d}x \quad i = 0, 1, 2, \ldots, \quad j = T, S, N \tag{3}$$

and have units of m^i/kg solvent. In (3), x (m) represents the one-dimensional length coordinate of the CSD and $n_j(x, t)$ (#/(kg m)) is the crystal size distribution at time, t.

The crystallization model is expressed in terms of the differential moment equations which track the progression of the moments of the CSD over the course of the crystallization. The total moments of the CSD are calculated from (4) and (5), and the seed moments are calculated from (6) and (7) by ignoring the influence of nucleation on the system.

$$\frac{\mathrm{d}\mu_{0,T}}{\mathrm{d}t} = B \tag{4}$$

$$\frac{\mathrm{d}\mu_{i,T}}{\mathrm{d}t} = iG\mu_{i-1,T} \quad i = 1, 2, 3, \ldots \tag{5}$$

$$\frac{\mathrm{d}\mu_{0,S}}{\mathrm{d}t} = 0 \tag{6}$$

$$\frac{\mathrm{d}\mu_{i,S}}{\mathrm{d}t} = iG\mu_{i-1,S} \quad i = 1, 2, 3, \ldots \tag{7}$$

In (4)–(7), B (#/(kg s)) and G (m/s) represent the secondary nucleation rate and crystal growth rate, respectively, and are expressed as empirical power law functions:

$$B = k_b S^b \mu_{3,T} \tag{8}$$

$$G = k_g S^g \tag{9}$$

where k_b (#/(m^3 s)) and b are nucleation parameters and k_g (m/s) and g are growth parameters that were estimated by Miller and Rawlings [2] for the potassium nitrate–water system. The estimated values along with their 95% confidence intervals are as follows: $\ln(k_b) = 26.863 \pm 0.360$, $b = 1.78 \pm 0.09$, $\ln(k_g) = -9.061 \pm 0.112$, and $g = 1.32 \pm 0.03$.

The supersaturation (ΔC) driving force for crystal growth and nucleation is expressed in terms of the relative supersaturation

$$S = \frac{\Delta C}{C^{sat}(T)} = \frac{C - C^{sat}(T)}{C^{sat}(T)} \tag{10}$$

where $C^{sat}(T)$ (kg solute/kg solvent) is the saturation concentration of potassium nitrate in water and is given by, $C^{sat}(T) = 0.1286 + 0.0058T + 0.0001721T^2$. T (°C) is the temperature and C (kg solute/kg solvent) is the concentration of potassium nitrate dissolved in water.

The system of equations is completed with a mass balance equation that describes the transfer of mass of the solute from the liquid phase to the solid phase

$$\frac{\mathrm{d}C}{\mathrm{d}t} = -3\rho_c G\mu_{2,T}. \tag{11}$$

The initial moments of the seed distribution were derived from the initial seed distribution, $n_S(x, 0) = \alpha f(x)$. Here, $f(x)$ (#/m) is an inverted polynomial distribution used by Chung et al. [6] and defined by, $f(x) = -[(x - \bar{L}(1 - W))][x - \bar{L}(1 + W)]$, $x \in [(\bar{L}(1 - W), \bar{L}(1 + W)]$. $\bar{L}$ (m) is the average length of the seed crystals and $W \in [0, 1]$ represents the dimensionless width of the seed distribution. α (1/kg) is a scalar factor defined by, $\alpha = m_{seed}/(\rho_c \mu_{3,f(x)})$, where m_{seed} (kg/kg) accounts for the mass of seed crystals per mass of solvent, ρ_c (kg/m^3) is the density of the crystals, and $\mu_{3,f(x)}$ (m^3) is the third moment of the inverted polynomial distribution. The parameter α accounts for the mass of seed crystals charged into the crystallizer at $t = 0$ and scales $f(x)$ accordingly.

We calculate the initial moments of this distribution using the initial seed distribution defined above and (3) (see (12)–(15)). Note that at $t = 0$, $\mu_{i,T} = \mu_{i,S}$.

$$\mu_{0,S}(0) = \frac{m_{seed}}{\rho_c} \frac{5}{\bar{L}^3(5 + 3W^2)} \tag{12}$$

$$\mu_{1,S}(0) = \frac{m_{seed}}{\rho_c} \frac{5}{\bar{L}^2(5 + 3W^2)} \tag{13}$$

$$\mu_{2,S}(0) = \frac{m_{seed}}{\rho_c} \frac{(5 + W^2)}{\bar{L}(5 + 3W^2)} \tag{14}$$

$$\mu_{3,S}(0) = \frac{m_{seed}}{\rho_c} \tag{15}$$

The following constraints were placed on the crystallization model and initial seed parameters: $\bar{L} = 0.6 \times 10^{-3}$ m, $W = 0.1$, $m_{seed} = 0.0231$ kg/kg, $t_b = 160$ min, $S(0) = 2.8 \times 10^{-3}$. The initial crystallizer temperature (T_i) was 32°C and the final temperature (T_f) was 22°C. The cooling rate was constrained between $(\mathrm{d}T/\mathrm{d}t)_{min} = -0.1$°C/min and $(\mathrm{d}T/\mathrm{d}t)_{max} = 0$°C/min.

3. Design of dynamic experiments

Design of experiments combined with response surface modeling is a data-driven approach for developing statistical models to characterize a process response through a set of statistically significant process variables. The process variables (x) are generally defined in terms of dimensionless (coded) variables (w),

$$x = x_{ref} + w\Delta x. \tag{16}$$

where $x_{ref} = (x_{max} + x_{min})/2$ and $\Delta x = (x_{max} - x_{min})/2$. x_{min} and x_{max} are the minimum and maximum values of the process variable being evaluated in the experimental design, respectively. The coded variable takes values between −1 and 1 depending on the type of experimental design chosen to evaluate the process. The main drawback of (16) in the DoE framework is its inability to evaluate time-variant process variables. This poses a problem for the data-driven optimization of batch processes, since batch processes are typically nonlinear and in general have time-varying optimal control trajectories.

Chen and Sheui [20] attempted to evaluate dynamic profiles using a data-driven technique. They presented a method that used a parameterized expansion of orthogonal basis functions to build a time-varying input trajectory and Taguchi's orthogonal array method to determine the number of basis functions to include in the profile and the parameter values that optimize the control trajectory. In a simulated environment, the authors applied the method to a penicillin model and found that 50 experiments were required to reach an optimum input trajectory. Georgakis [1] independently developed an experimental design methodology that provides a systematic way to design experiments with time-varying input trajectories for batch processes. His design of dynamic experiments methodology formulates dynamic input trajectories in a similar fashion to (16) and uses the approach of DoE to determine the experimental design points. His systematic approach requires a smaller number of experiments, which is of critical importance in an experimental design methodology. As stated earlier, when DoDE is combined with RSM and linear/nonlinear optimization it yields a data-driven optimization technique called DoDE optimization.

In what follows, we demonstrate how DoDE, as a data-driven methodology, allows for the systematic evaluation of time-varying profiles using the techniques of design of experiments and response surface modeling. The dynamic variable $u(\tau)$ is approximated

by $u_n(\tau)$ which is expressed in terms of a finite basis function expansion around a reference trajectory ($u_{ref}(\tau)$)

$$u(\tau) \approx u_n(\tau) = u_{ref}(\tau) + \Delta u(\tau) \sum_{i=1}^{n} a_i \phi_i(\tau) \tag{17}$$

where $u_{ref}(\tau) = (u_{max}(\tau) + u_{min}(\tau))/2$ and $\Delta u = (u_{max}(\tau) - u_{min}(\tau))/2$. $u_{min}(\tau)$ and $u_{max}(\tau)$ are the lower and upper bounds of the trajectories of interest, respectively, and τ is the dimensionless time, defined by $\tau = t/t_b$. The coefficients a_i, referred to as dynamic subfactors (DSF), play the same role as coded variables in the DoE case in terms of defining a design space[1] and acting as regressors in the RSM. Upon further inspection of (17) we find that (16) is a special case, specifically, when $u_{ref}(\tau)$ and $\Delta u(\tau)$ have no τ dependence, $n = 1$, $\phi_1(\tau) = 1$, and $a_1 = w$.

For this study, the cooling rate profile was parameterized as an expansion of shifted Legendre polynomials. The cooling rate profile was selected in order to satisfy the cooling rate constraints placed on the crystallization. The temperature profile was then obtained by integrating the cooling rate profile. The shifted Legendre polynomials were selected as they represent a complete set of orthogonal polynomial functions in the interval [0, 1]. This allows for evaluation of the time-variant cooling rate profiles over the dimensionless time interval [0, 1]. The general expansion for the dimensionless cooling rate equation is

$$-u_n(\tau) = -\frac{d\theta}{d\tau} = 1 + \sum_{i=1}^{n} a_i P_i(\tau). \tag{18}$$

Comparing (18) to (17) we see that $u_{ref}(\tau) = 1$ and $\Delta u = 1$. $P_i(\tau)$ is the ith shifted Legendre polynomial and a_i is the ith dynamic subfactor. Here, θ is the dimensionless temperature ($\theta = (T - T_i)/(T_i - T_f)$). Setting $u_{ref}(\tau) = 1$ forces the temperature profile at $t = 0$ and $t = t_b$ to take the values T_i and T_f, respectively.

For the case of two dynamic subfactors ($n = 2$), the dimensionless cooling rate is parameterized as

$$\frac{d\theta}{d\tau} = -1 - a_1(2\tau - 1) - a_2(1 - 6\tau + 6\tau^2). \tag{19}$$

Integrating (19) gives the dimensionless temperature profile

$$\theta(\tau) = -\tau - a_1(\tau^2 - \tau) - a_2(\tau - 3\tau^2 + 2\tau^3). \tag{20}$$

The design space for the dynamic subfactors is determined by enforcing the cooling rate constraints on the cooling rate profile. In dimensionless form the constraint is

$$-1.6 \le \frac{d\theta}{d\tau} \le 0 \quad \tau \in [0, 1]. \tag{21}$$

The design space is represented by the intersection of inequalities (22)–(24).

$$-1.6 \le \frac{d\theta(0)}{d\tau} \le 0 \tag{22}$$

$$-1.6 \le \frac{d\theta(1)}{d\tau} \le 0 \tag{23}$$

$$-1.6 \le \frac{d\theta(\tau^*)}{d\tau} \le 0 \quad \tau^* \in [0, 1] \tag{24}$$

[1] The term *design space* in this manuscript represents the set of allowable values of the variables in the experimental design. It does not refer to the FDA's definition of design space.

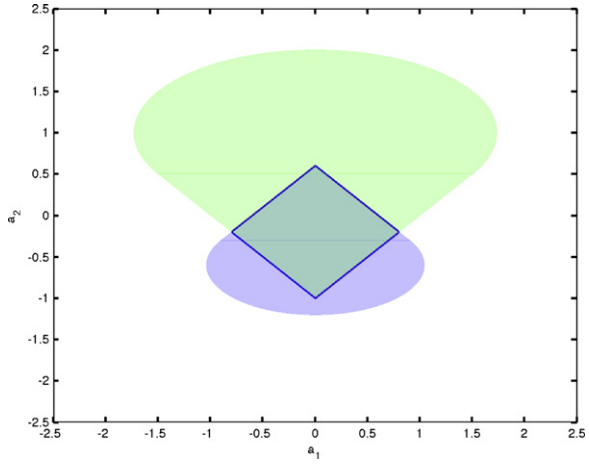

Fig. 1. Design space inequalities (22)–(24) for the two dynamic subfactor case. The design space is defined as the intersection of the inequalities, in this case the diamond region in the center of the figure.

The variable τ^* in (24) denotes the time instance at which the cooling rate attains a minimum or maximum value and is found by solving (25) for τ.

$$\frac{d}{d\tau}\left(\frac{d\theta}{d\tau}\right) = 0 \tag{25}$$

Inequalities (22) and (23) limit the value of the cooling rate at $t = 0$ and $t = t_b$, respectively, and impose linear constraints on the dynamic subfactors. Inequality (24) has the potential to generate nonlinear bounding constraints on the dynamic subfactors when dealing with polynomial basis functions of order two and higher.

The area bound by inequalities (22)–(24) with (19) is shown in Fig. 1. The nonlinear boundaries generated from (24) are depicted by the curved lines. Only the intersection of the inequalities is active in defining the design space. In Fig. 1, the design space is represented by the diamond-shaped intersection and specified by the following four linear inequalities.

$$-a_1 + a_2 \le 0.6 \tag{26}$$

$$a_1 + a_2 \le 0.6 \tag{27}$$

$$a_1 - a_2 \le 1 \tag{28}$$

$$-a_1 - a_2 \le 1 \tag{29}$$

The intersection of (26)–(29) is expanded in Fig. 2. The solid circles in Fig. 2 represent design points where experiments will be performed to evaluate the two response variables of interest, m_0 (1) and m_3 (2), within the design space. For this design space, we used a central composite design to select the location of the design points. Figs. 3 and 4 depict the dimensionless cooling rate and temperature trajectories, respectively, for five of the nine experimental design points. Note that all cooling rates satisfy (21) and all temperature trajectories generated from points inside the design space are bound from above and below by the temperature profiles generated at design points $(a_1, a_2) = (0.8, -0.2)$ and $(-0.8, -0.2)$, respectively.

As mentioned earlier, the function selected for the parameterized input profile can limit the range of values the profile can achieve. The lower cooling rate constraint that can be evaluated using the parameterized cooling rate profile (18) depends on the number of basis functions included in the expansion. Suppose the lower cooling rate constraint was −0.5°C/min instead of −0.1°C/min. Evaluation of (18) with two basis functions yields a minimum cooling rate of −0.25°C/min, three basis functions yields a cooling rate of −0.375°C/min, and four basis functions yields −0.56°C/min. This suggests that at least four basis functions, and

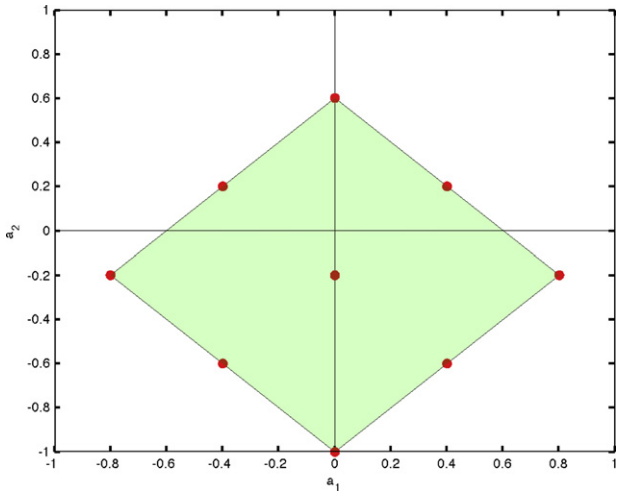

Fig. 2. Design space for two dynamic subfactors. Experimental points are denoted by solid circles.

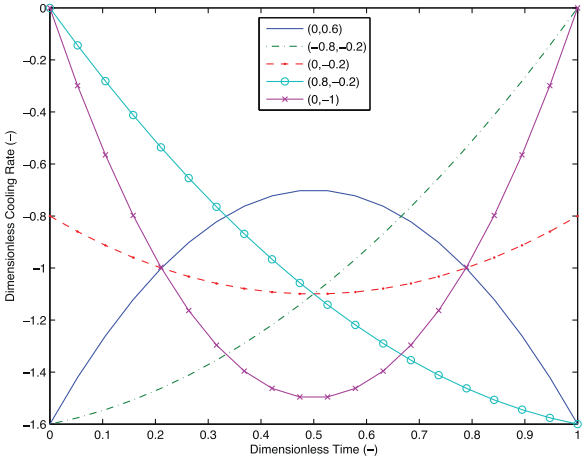

Fig. 3. Cooling rate profiles generated using five of the nine design points from within the design space shown in Fig. 2.

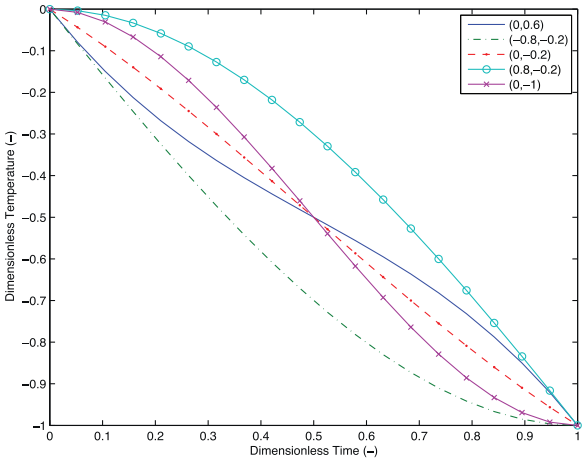

Fig. 4. Temperature profiles generated using five of the nine design points from within the design space shown in Fig. 2. These temperature trajectories correspond to the cooling rate profiles shown in Fig. 3.

four dynamic subfactors, are required to evaluate cooling rates down to −0.5°C/min. It also shows that the number of dynamic subfactors required in the experimental design, and the number of experiments that must be performed, increases when evaluating systems with decreasing cooling rate constraints.

4. Results and discussion

We now apply the DoDE optimization technique to the seeded, potassium nitrate–water batch crystallization model discussed in Section 2 and compare the results of the optimum temperature profiles calculated for (1) and (2) to the temperature profiles calculated using a model-based optimization technique.

4.1. Model-based optimization

The model-based optimum temperature profile was determined by solving the following nonlinear optimization problem:

$$\begin{aligned} &\min_{T(t)} \quad J(t_b) \\ &\text{s.t.} \quad \text{model Eqs.: (4)–(11)} \\ &\qquad \text{initial seed conditions: (12)–(15)} \\ &\qquad \text{constraints :} \\ &\qquad T_f \le T \le T_i \\ &\qquad \left(\frac{dT}{dt}\right)_{min} \le \frac{dT}{dt} \le \left(\frac{dT}{dt}\right)_{max} \end{aligned} \tag{30}$$

where $J(t_b) = m_0$ for the first objective (1) and $J(t_b) = -m_3$ for the second objective (2). The model parameter values and initial condition values for (4)–(15) and the constraint values are listed in Section 2.

The crystallization model was converted to a system of algebraic equations using Radau collocation on finite elements [18]. The system was discretized into 15 finite elements with 3 collocation points per element. Before performing the optimization, the crystallization model was integrated using an arbitrary temperature trajectory so that the optimization routine would begin on a constraint manifold. In order to ensure a global optimum was found, the optimization routine was run using a number of different initial temperature profiles. In all cases they converged to the results reported.

We solved the model-based optimization problem using the general algebraic modeling system (GAMS) [21] and the nonlinear, constrained optimization solver, SNOPT [22], on the NEOS Server for Optimization [23–25].

For the first objective, minimize m_0, the optimum value was found to be 64.89. The resulting optimum temperature profile is shown in Fig. 5. For the second objective, maximize m_3, the optimum value was found to be 1.683. The resulting optimum temperature profile is shown in Fig. 6.

4.2. Design of dynamic experiments optimization

The experimental data required to implement the DoDE optimization strategy was simulated using the crystallization model in Matlab [26] using the Runge–Kutta solver *ode45*. In order to introduce variability into the simulated results, a normally distributed random error not greater than 2%, $N(0, 0.02/3)$, of the simulated value was added to the response variables, m_0 and m_3, at the end of each simulated experiment.

4.2.1. Two dynamic subfactors

In order to calculate the optimum values of the dynamic subfactors, a_1 and a_2, in the parameterized cooling rate function (19), data were simulated at each of the experimental points shown in Fig. 2 for responses (1) and (2). In addition to these nine data

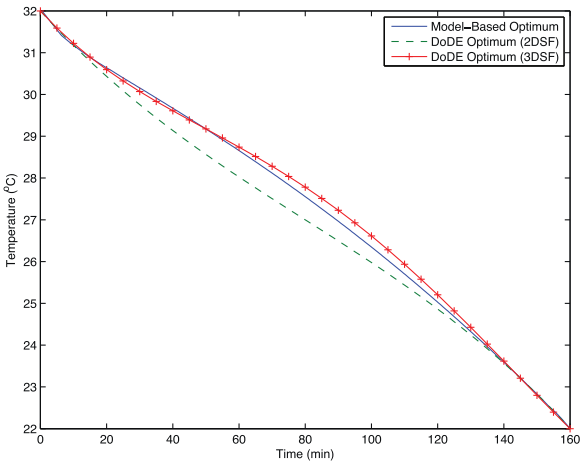

Fig. 5. Optimum temperature profiles for objective minimize m_0.

points, three additional center-point experiments were simulated. The replicated center-point experiments were used to estimate the inherent variability of the process, which was assumed to be uniform throughout the design space. This value was used to determine the significance of each term in the response surface model and to calculate the lack of fit (LoF) statistic. The LoF statistic was used to evaluate whether the response surface model adequately represented the variability in the data that was not attributed to the inherent variability.

Second-order response surface models were fitted to the simulated response variables, m_0 and m_3. Before estimating the model parameters, the dynamic subfactors were scaled to range between −1 and 1 with the following scaling function

$$\bar{a} = \frac{a - (a_{max} + a_{min})/2}{(a_{max} - a_{min})/2} \tag{31}$$

where $\bar{a}$ is the scaled variable, and where a_{min} and a_{max} are the minimum and maximum values of the dynamic subfactor. For the two dynamic subfactor case the variable scalings are

$$\bar{a}_1 = \frac{a_1}{0.8} \tag{32}$$

$$\bar{a}_2 = \frac{a_2 + 0.2}{0.8}. \tag{33}$$

This scaling was performed so the magnitude of significant parameter estimates was of the same order and so each parameter estimate was made with similar precision [15].

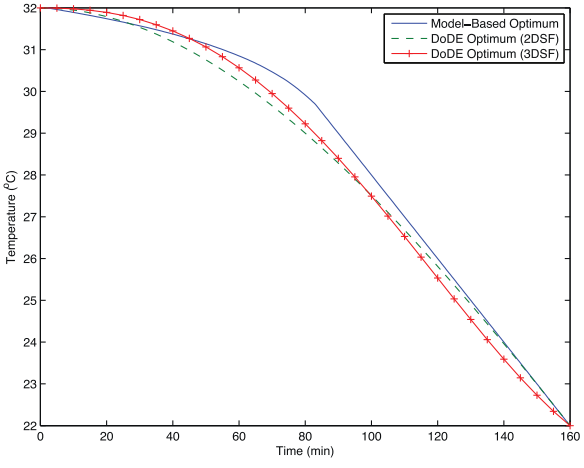

Fig. 6. Optimum temperature profiles for objective maximize m_3.

Table 1
RSM parameter estimates and 95% confidence intervals with VIF for 2 DSF models.

Parameter	Response m_0		Response m_3	
	Estimate	VIF	Estimate	VIF
$\hat{\beta}_0$	65.83 ± 0.54	–	1.488 ± 0.009	–
$\hat{\beta}_1$	0	–	0.143 ± 0.011	1
$\hat{\beta}_2$	-1.88 ± 0.68	1	-0.063 ± 0.011	1
$\hat{\beta}_{12}$	0	–	0	–
$\hat{\beta}_{11}$	3.94 ± 1.02	1.13	0.023 ± 0.017	1.13
$\hat{\beta}_{22}$	1.28 ± 1.02	1.13	-0.027 ± 0.017	1.13

A second-order response surface model is defined by

$$\hat{y} = \hat{\beta}_0 + \sum_{i=1}^{n} \hat{\beta}_i \bar{a}_i + \sum_{i=1}^{n} \sum_{j=i+1}^{n} \hat{\beta}_{ij} \bar{a}_i \bar{a}_j + \sum_{i=1}^{n} \hat{\beta}_{ii} \bar{a}_i^2 \tag{34}$$

where $\hat{y}$ is the predicted response (objective) variable, in this case m_0 or m_3, and $\hat{\beta}_i$, $\hat{\beta}_{ij}$, and $\hat{\beta}_{ii}$ are the model parameters.

Second-order response surface models were fitted to the data for each response variable using linear least squares regression. Models and parameter estimates were tested at a significance level of $\alpha = 0.05$. The parameter estimates and 95% confidence intervals for the m_0 and m_3 response surface models are listed in Table 1. Parameters whose confidence intervals included zero are nonsignificant and denoted in Table 1 with a zero value. The significance of the parameter estimates was evaluated using a partial t-test.

The following steps were taken to test the validity of each response surface model: (1) the variance inflation factors (VIF) were calculated to determine if multicollinearity existed between regressors; (2) the model residuals were calculated to ensure they were normally distributed; (3) the adjusted R^2 (R^2(adj)) and predicted R^2 (R^2(pred)) values were calculated to determine how much of the variability in the data was explained and predicted by the RSM; and (4) the lack of fit statistics were calculated for each RSM to ensure the model adequately fit the data.

The VIF values reported in Table 1 indicate the amount of multicollinearity between regressors, in this case the dynamic subfactors, in the model. A value of one indicates no multicollinearity, while values above 10 indicate the presence of multicollinearity between two or more of the regressors [16]. Multicollinearity leads to parameters estimates with large standard errors and models with poor predictive capabilities. The VIF values for the parameters in the two RSM models have values of one or close to one indicating the regressors are not correlated.

An evaluation of the model residuals (data not presented) found them to be structureless and normally distributed. No patterns in the data were seen when the residuals were plotted versus the predicted response or against experiment number. The Shapiro–Wilk W test was used to evaluate whether the model residuals were distributed normally for each response. In both cases the test statistic had a p-value >0.05 indicating that the null hypothesis, the residuals are normally distributed, could not be rejected.

R^2(adj) and R^2(pred) values for each RSM model are listed in Table 2. Values close to 100% are desired. The R^2(adj) value describes how much of the variability in the response data is accounted for by the model. It is similar to the R^2 statistic but is corrected for the number of factors in the model, making it a better indication of how the variability in the data is accounted for. In the case of the m_0 and m_3 RSM's, we see that 91% and 99% of the variability in the data is accounted for by each model, respectively.

The R^2(pred) value is an indication of how much of the variability in the predicted response is accounted for by the RSM. The R^2(pred) values for the m_0 and m_3 RSM's indicate that the models will account for 84% and 98% of the variability, respectively, when using the model to predict outcomes within the design space.

Table 2
DoDE results summary.

Response	Number of experiments	R^2(adj)	R^2(pred)	LoF p-value	Optimum values			Predicted response	Simulated response
					a_1	a_2	a_3		
m_0 (2 DSF)	12	0.91	0.84	0.70	0	0.39	–	65.14 ± 1.29	65.39
m_3 (2 DSF)	12	0.99	0.98	0.76	0.80	−0.20	–	1.653 ± 0.023	1.634
m_0 (3 DSF)	21	0.96	0.94	0.97	0.24	0.32	−0.31	65.06 ± 0.84	65.08
m_3 (3 DSF)	21	0.96	0.91	0.63	0.81	−0.49	−0.30	1.663 ± 0.036	1.631

The LoF statistic was calculated by splitting the sum of the square of the errors for the RSM into a pure error and lack of fit component. The pure error is calculated using the replicated center-point experiments, four in this work, making it independent of the error in the RSM. The lack of fit error is calculated from residuals found using the overall average predicted response and the individual predicted responses at each experimental point. The lack of fit statistic follows an F-distribution, therefore, if the ratio of the mean square of pure error to mean square of LoF error is close to one, the lack of fit statistic is not significant (p-value >0.05), indicating the model is not missing any significant terms. The LoF statistic for each model is presented in Table 2. Each RSM has a lack of fit statistic that is nonsignificant, indicating that the form of the RSM adequately describes the data for each response variable.

The following optimization problem was solved in order to find the optimum values of the dynamic subfactors that minimized and maximized the response surface model representing m_0 and m_3, respectively:

$$\begin{aligned} \min_{\bar{a}_1,\bar{a}_2} \quad & \hat{y}(34) \\ \text{s.t.} \quad & \hat{\beta} \text{ values listed in Table 1} \\ & \text{design space constraints (26)–(29)} \end{aligned} \tag{35}$$

where $\hat{y} = m_0$ for the fist objective and $\hat{y} = -m_3$ for the second objective.

The optimum values of the dynamic subfactors were used to calculate the predicted responses and 95% prediction intervals for both the m_0 and m_3 response surface models. Optimum temperature profiles were generated from (20) using the optimum dynamic subfactor values for each RSM. The crystallization model was simulated to determine the value of m_0 and m_3 using the appropriate optimized temperature trajectory. The predicted response values found using the RSM's agree with the simulated values calculated using the optimum temperature trajectories. The optimum dynamic subfactors, predicted response, and simulated response values are reported in Table 2.

Results of the optimized objectives are given in Table 4. The values reported for the DoDE optimization method were obtained by simulating the crystallization model using the optimum temperature trajectory generated from the optimum dynamic subfactor values. It is seen that the DoDE optimization is able to calculate an optimum operating trajectory that comes within 0.77% of the model-based optimum for the objective minimize m_0 and within 2.9% of the model-based optimum for the objective maximize m_3.

In order to get a sense of the variability in the response data from the DoDE simulations, the percent difference between the model based optimum and the least favorable experimental result for each response variable was calculated. Evaluating the response variable m_0, the least favorable temperature trajectory was located at (−0.8, −0.2) where m_0 = 69.98 and the percent difference from the model based optimum was 7.8%. For response m_3, the least favorable trajectory was also located at (−0.8, −0.2) where m_3 = 1.367 and the percent difference from the model based optimum was 18.8%. The temperature profile generated at (a_1, a_2) = (−0.8, −0.2) is similar to a natural cooling (temperature) profile (see Fig. 4), which have been reported [8,27] to increase nucleation in the early stages of the crystallization due to elevated supersaturation values generated by the elevated initial rate of cooling.

Table 3
RSM parameter estimates and 95% confidence intervals with VIF for 3 DSF models.

Parameter	Response m_0		Response m_3	
	Estimate	VIF	Estimate	VIF
$\hat{\beta}_0$	65.91 ± 0.34	–	1.491 ± 0.009	–
$\hat{\beta}_1$	0	–	0.128 ± 0.015	1.65
$\hat{\beta}_2$	−2.04 ± 0.36	1.06	−0.072 ± 0.015	1.10
$\hat{\beta}_3$	1.25 ± 0.36	1.05	0.041 ± 0.018	1.49
$\hat{\beta}_{12}$	−2.30 ± 0.76	1.10	0	–
$\hat{\beta}_{13}$	0	–	−0.078 ± 0.050	2.12
$\hat{\beta}_{23}$	0	–	0.056 ± 0.040	1.14
$\hat{\beta}_{11}$	2.92 ± 0.50	1.06	0	–
$\hat{\beta}_{22}$	2.05 ± 0.61	1.14	0	–
$\hat{\beta}_{33}$	1.96 ± 0.55	1.09	−0.052 ± 0.030	1.93

4.2.2. Three dynamic subfactors

The two dynamic subfactor DoDE design was augmented with nine additional experimental points in order to evaluate a cooling rate profile with three dynamic subfactors

$$\frac{d\theta}{d\tau} = -1 - a_1(2\tau - 1) - a_2(1 - 6\tau + 6\tau^2) - a_3(20\tau^3 - 30\tau^2 + 12\tau - 1). \tag{36}$$

The design space was calculated using (22)–(25) with (36) and was found to have an active, nonlinear bounding surface constraint. Therefore, a D-optimal experimental design algorithm was used to augment the 2 DSF experimental design with nine additional experimental points. The dynamic subfactors were once again scaled to range between −1 and 1 using (31) and a second-order RSM was fit to the simulated response data. The RSM's were analyzed in the same manner as before. Parameter estimates and VIF values are presented in Table 3 and a summary of the model and optimization results are presented in Table 2. A comparison of the DoDE optimization results for the 3 DSF design versus the model-based optimization results are presented in Table 4.

Evaluation of the results presented in Table 2 shows that for the response m_0 an improvement is seen in the objective value when moving from 2 DSF to 3 DSF. This improvement is also seen

Table 4
DoDE versus model-based optimum.

	Objectives	
	min m_0	max m_3
Model-based optimum (MBO)	64.89	1.683
DoDE optimum (2 DSF)	65.39	1.634
% Difference from MBO (2 DSF)	0.77%	2.91%
DoDE optimum (3 DSF)	65.08	1.631
% Difference from MBO (3 DSF)	0.29%	3.09%

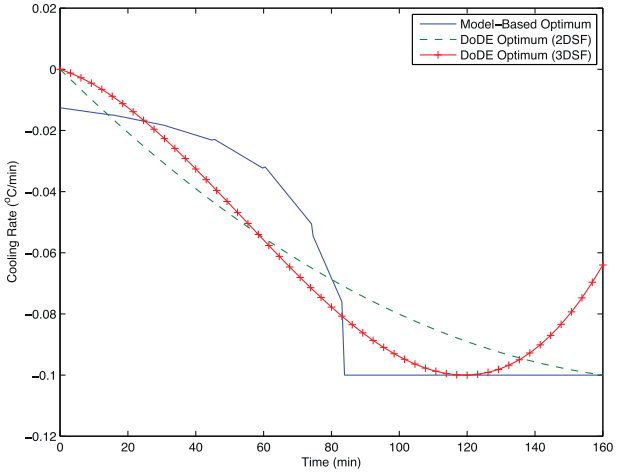

Fig. 7. Optimum cooling rate profiles for objective maximize m_3.

in the agreement between the optimum DoDE and MBO temperature profiles (Fig. 5). While an improvement is seen between the 2 DSF and 3 DSF cases it is modest and the cost associated with running nine additional experiments to fit the third DSF may not be worth the effort. This is quantified in the predicted response data as there is not a significant difference between the 2 DSF and 3 DSF predictions.

The results for response m_3 show that there is essentially no difference in the objective values obtained from the optimal temperature trajectories calculated from the 2 DSF and 3 DSF response surface models. Evaluation of the optimal temperature profiles in Fig. 6 shows no real improvement in the optimal trajectory with the addition of a third DSF. In order to gain a better understanding of why no improvement was seen, the optimal cooling rate trajectories were plotted for the MBO and 2 DSF and 3 DSF cases (Fig. 7). The optimal cooling rate trajectory for the MBO was found to be piecewise continuous, consisting of a singular arc followed by a segment where the cooling rate attains its maximum negative value of -0.1°C/min.

The form of the MBO cooling rate trajectory cannot be obtained using 2 or 3 DSF since the derivatives of the DoDE temperature and cooling rate profiles are always continuous. Therefore, in order to approximate the MBO temperature profile with high accuracy a large number of basis functions are required in the expansion of (18). The number of basis functions required can be determined by projecting the optimal cooling rate profile onto the basis functions in order to find a function in the span of the basis function space which approximates the MBO cooling rate profile. Doing so reveals that >20 basis functions are required to generate a profile that begins to approximate the MBO profile in Fig. 7. Evaluating 20 DSF is an experimentally exorbitant undertaking.

It is well known that the near optimal temperature trajectories for batch cooling crystallizations follow trajectories similar to the one obtained for objective m_3 [8]. Temperature trajectories of this form, slow cooling followed by fast cooling, have also been found experimentally for cooling crystallizations operated under concentration control at a constant supersaturation set point [28]. One option for improving upon the DoDE profiles tested in this analysis would be to break the time interval into two subintervals using a switch time (τ_s) variable. Setting the cooling rate in the second time interval ($\tau \in [\tau_s, 1]$) at the most negative cooling rate attainable by the crystallizer, the dimensionless switch temperature (θ_s) could be calculated at τ_s. Using this information, DoDE profiles ($u_n(\tau)$) for the cooling rate could be designed on the interval $\tau \in [0, \tau_s)$ and a set of experiments could be generated to evaluate the values of the dynamic subfactors in $u_n(\tau)$ along with the value for τ_s.

Table 5
RSM parameter estimates and 95% confidence intervals with VIF for 2 DSF models simulated using random differential equations.

Parameter	Case 1		Case 2	
	Estimate	VIF	Estimate	VIF
$\hat{\beta}_0$	1.461 ± 0.014	–	1.463 ± 0.038	–
$\hat{\beta}_1$	0.139 ± 0.028	1	0.162 ± 0.075	1
$\hat{\beta}_2$	−0.062 ± 0.028	1	−0.110 ± 0.075	1

For both objectives evaluated here, DoDE was able to find optimum values within a few percent of the model-based optimum values. In most cases, the true optimum is unknown and the DoDE approximation to the true optimum using 2 or 3 DSF will be adequate. This will be shown in the next section by performing a sensitivity analysis around the model-based optimum temperature profile and the DoDE optimum profile with 2 DSF.

4.3. Sensitivity analysis

Stochastic simulations were performed to evaluate the sensitivity of the system response around the optimum temperature profile to variability in the process parameters. This was achieved by simulating the crystallization model using random parameter values following an approach used by Lal Tiwari and Hobbie [29]. This sensitivity analysis aims to help us understand how the response variable m_3 is affected by the uncertainty in the model parameters for both the MBO and DoDE optimum temperature trajectories. The nucleation and growth rate parameter estimates and 95% confidence intervals calculated by Miller and Rawlings [2], and reported in Section 2, were assumed to come from a normal distribution. Each parameter had a mean (p_μ) and standard deviation (p_σ). Random parameter values (p) for each of the model parameters were sampled from $p = p_\mu + p_\sigma N(0, 1)$ where $N(0, 1)$ is a normally distributed random variable with mean equal to zero and standard deviation equal to one.

A fixed-step Runge–Kutta solver was implemented in Matlab using vectorized code in order to enable a large number of stochastic simulations (realizations) of the crystallization model in a short amount of time. The system was simulated for two cases

- Case 1: Random parameter values and fixed initial seed conditions.
- Case 2: Random parameter values and random initial seed conditions.

In both cases, the random parameter values were sampled and updated at each time step in the numerical integration. In Case 2, randomness was also introduced in the initial moment equations for the seed distribution (12)–(15) through $\bar{L}$ and W at $t = 0$. The average seed length $\bar{L}$ was assumed to have mean $\bar{L}_\mu = 0.6 \times 10^{-3}$ m and standard deviation $\bar{L}_\sigma = 0.1 \times 10^{-4}$ m. The width of the seed distribution W was assumed to have mean $W_\mu = 0.1$ and standard deviation $W_\sigma = 0.01$. The random variables, $\bar{L}$ and W, were assumed to come from a normal distribution.

Temperature profiles that optimized the response m_3 were calculated using the DoDE optimization method for Cases 1 and 2 of the stochastic system with the two dynamic subfactor design (Fig. 2) and a second-order response surface model. The optimum values of the dynamic subfactors were again calculated to be $(a_1, a_2) = (0.8, -0.2)$ for both Cases 1 and 2. Only the intercept and first order terms were found to be significant in both RSM's (see Table 5). The model statistics for Case 1 were $R^2(\text{adj}) = 0.93$ and LoF = 0.87. The model statistics for Case 2 were $R^2(\text{adj}) = 0.74$ and LoF = 0.07.

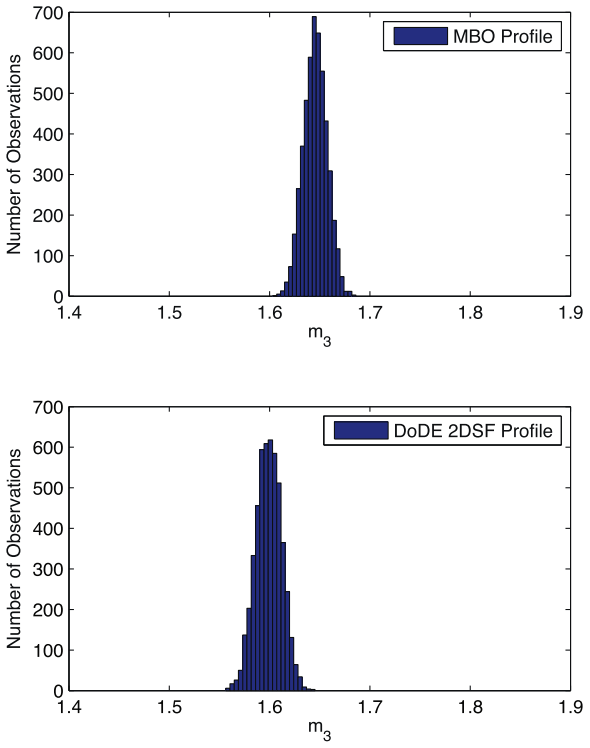

Fig. 8. Crystallization model simulated 5000 times with error in the parameters using the MBO temperature profile (top) and the DoDE optimum temperature profile (bottom).

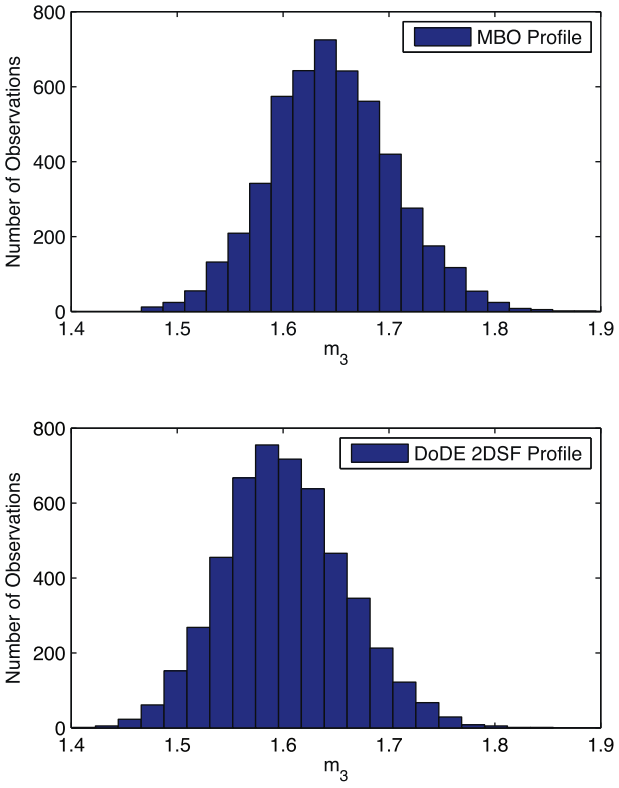

Fig. 9. Crystallization model simulated 5000 times with error in the parameters and initial seed conditions using the MBO temperature profile (top) and the DoDE optimum temperature profile (bottom).

The R^2(adj) statistic indicates that the RSM for Case 2 is not able to account for the variability in the data as well as in Case 1. The lack of fit statistic for Case 2 is also much smaller than the LoF for Case 1. This is due to the increase in inherent variability in the data caused by the random initial seed conditions simulated in Case 2. Also, the fact that only the intercept and first order terms are significant in the RSM's brings up the point that the experimental analysis should proceed sequentially, especially in the present case where the design space is fixed and cannot be moved. If real experiments were being performed, it would have been more advisable to run experiments at the corner points of the design space, with replicated center points, and fit a first order RSM to the measured response data. The LoF statistic could then be used to determine if a second order model was more appropriate and the experimental analysis could be augmented with additional experimental points.

To understand how the response variable m_3 was distributed in the presence of parameter and initial seed condition uncertainty, 5000 simulations were preformed using the MBO and DoDE optimum temperature profiles for Cases 1 and 2. The model based optimum temperature profile calculated previously for the m_3 objective was again taken as the true reference optimum. The DoDE optimum temperature profile was generated using the optimum dynamic subfactor values $(a_1, a_2) = (0.8, -0.2)$ for each of the RSM's calculated from Cases 1 and 2.

Histograms for m_3 are shown in Figs. 8 and 9 for Case 1 and Case 2, respectively. Fig. 8 shows that when only parameter variability is accounted for the values of m_3 are tightly distributed around the distribution mean. Fig. 9 shows that the variability in the distribution of m_3 is greatly increased when the model is simulated with randomness in the initial seed condition. Based on these results, it appears the outcome of the crystallization is much more sensitive to the initial seed characteristics than to variability in the kinetic parameters.

The power of the DoDE methodology is clearly seen in the results of Case 2 where there is large overlap in the two distributions for m_3. Here we see that the optimum temperature profile obtained using DoDE yields results from a distribution that is very close to the distribution obtained with the model based temperature profile. Since all processes have some amount of inherent variability, these simulations show that while DoDE does not find the true optimum dynamic profile, it is able to find a near optimal profile that generates results almost equivalent to those from a true optimum profile once process variability is accounted for.

5. Conclusions

In this paper we showed how the design of dynamic experiments optimization methodology can be used to optimize a time-variant input profile for a simple, batch crystallization process without the need for a first-principles model. The DoDE methodology was capable of finding near optimal temperature trajectories for early and late-growth optimization objectives that resulted in objective values within a few percent of the model-based optimum.

It was seen that for smooth cooling rate profiles, the addition of a third dynamic subfactor improved the optimization objective. However, when the cooling rate profile had a discontinuity in its derivative, the addition of a third dynamic subfactor resulted in no improvement in the value of the optimization objective. More work needs to be done to address how the DoDE methodology can be used to determine if a profile is piecewise continuous and how best to modify the experimental design.

The sensitivity analysis showed that when random variability in the parameter values and initial seed conditions was accounted for in the model, there was a large amount of overlap in the distributions of the response variable for the model-based and DoDE optimum temperature trajectories. This result indicates that

this crystallization model is highly sensitive to the initial seed characteristics, and more importantly, that in the presence of process variability there is little difference in the distributions of the response variable between the true optimum input trajectory and the near-optimum DoDE trajectory. Further simulation work must be performed which considers plant/model mismatch in order to give a more realistic comparison between DoDE optimization and model-based optimization.

Based on the findings presented in this paper, the DoDE optimization methodology has the potential to be extremely useful for optimizing complex batch crystallization processes where no first-principles model exists or where the response variable to be optimized cannot be expressed in terms of a first-principles model.

Acknowledgement

We would like to thank Jacob Sizemore for his helpful discussions while writing this manuscript.

References

[1] C. Georgakis, A model-free methodology for the optimization of batch processes: design of dynamic experiments, in: Proceedings of the 7th IFAC International Symposium on Advanced Control of Chemical Processes (ADCHEM), Istanbul, Turkey, 2009.
[2] S.M. Miller, J.B. Rawlings, Model identification and control strategies for batch cooling crystallizers, AIChE Journal 40 (1994) 1312–1327.
[3] Z.K. Nagy, M. Fujiwara, R.D. Braatz, Modelling and control of combined cooling and antisolvent crystallization processes, Journal of Process Control 18 (2008) 856–864.
[4] J. Worlitschek, M. Mazzotti, Model-based optimization of particle size distribution in batch-cooling crystallization of paracetamol, Crystal Growth & Design 4 (2004) 891–903.
[5] Q. Hu, S. Rohani, A. Jutan, Modelling and optimization of seeded batch crystallizers, Computers & Chemical Engineering 29 (2005) 911–918.
[6] S.H. Chung, D.L. Ma, R.D. Braatz, Optimal seeding in batch crystallization, Canadian Journal of Chemical Engineering 77 (1999) 590–596.
[7] Y. Lang, A.M. Cervantes, L.T. Biegler, Dynamic optimization of a batch cooling crystallization process, Industrial & Engineering Chemistry Research 38 (1999) 1469–1477.
[8] J.W. Mullin, J. Nyvlt, Programmed cooling of batch crystallizers, Chemical Engineering Science 26 (1971) 369–377.
[9] J.D. Ward, D.A. Mellichamp, M.F. Doherty, Choosing an operating policy for seeded batch crystallization, AIChE Journal 52 (2006) 2046–2054.
[10] K.L. Choong, R. Smith, Optimization of batch cooling crystallization, Chemical Engineering Science 59 (2004) 313–327.
[11] D. Sarkar, S. Rohani, A. Jutan, Multi-objective optimization of seeded batch crystallization processes, Chemical Engineering Science 61 (2006) 5282–5295.
[13] T. Togkalidou, R.D. Braatz, B.K. Johnson, O. Davidson, A. Andrews, Experimental design and inferential modeling in pharmaceutical crystallization, AIChE Journal 47 (2001) 160–168.
[14] A. Fiordalis, C. Georgakis, Design of dynamic experiments versus model-based optimization of batch crystallization processes, in: Proceedings of the 18th World Conference of the International Federation of Automatic Control (IFAC), Milano, Italy, 2011.
[15] D.C. Montgomery, Design and Analysis of Experiments, 6th ed., John Wiley & Sons, Inc., Hoboken, New Jersey, 2005.
[16] R.H. Myers, D.C. Montgomery, Response Surface Methodology: Process and Product Optimization Using Design of Experiments, John Wiley & Sons, Inc., New York, New York, 1995.
[17] T.F. Edgar, D.M. Himmelblau, L.S. Lasdon, Optimization of Chemical Processes, McGraw-Hill Chemical Engineering Series, 2nd ed., McGraw-Hill, New York, New York, 2001.
[18] L.T. Biegler, A.M. Cervantes, A. Wächter, Advances in simultaneous strategies for dynamic process optimization, Chemical Engineering Science 57 (2002) 575–593.
[19] H.M. Hulburt, S. Katz, Some problems in particle technology: a statistical mechanical formulation, Chemical Engineering Science 19 (1964) 555–574.
[20] J. Chen, R.G. Sheui, Using Taguchi's method and orthogonal function approximation to design optimal manipulated trajectory in batch processes, Industrial & Engineering Chemistry Research 41 (2002) 2226–2237.
[21] General Algebraic Modelling System (GAMS), version 23.7.3, GAMS Development Corporation, Washington, DC, 2011.
[22] P.E. Gill, W. Murray, M.A. Saunders, SNOPT: an SQP algorithm for large-scale constrained optimization, SIAM Review 47 (2005) 99–131.
[23] J. Czyzyk, M.P. Mesnier, J.J. Moré, The NEOS server, Computational Science & Engineering, IEEE 5 (1998) 68–75.
[24] W. Gropp, J.J. Moré, Optimization environments and the NEOS server, in: M.D. Buhmann, A. Iserles (Eds.), Approximation Theory and Optimization, Cambridge University Press, Cambridge, United Kingdom, 1997, pp. 167–182.
[25] E.D. Dolan, NEOS Server 4.0 Administrative Guide, Technical Memorandum 250, Argonne National Laboratory, Argonne, Illinois, 2001.
[26] MATLAB, version 7.12.0.635 (R2011a), The Mathworks Inc., Natick, MA, 2011.
[27] R.J. Davey, J. Garside, From Molecules to Crystallizers, Oxford University Press, Oxford, United Kingdom, 2000.
[28] V. Liotta, V. Sabesan, Monitoring and feedback control of supersaturation using ATR–FTIR to produce an active pharmaceutical ingredient of a desired crystal size, Organic Process Research & Development 8 (2004) 488–494.
[29] J. Lal Tiwari, J.E. Hobbie, Random differential equations as models of ecosystems: Monte Carlo simulation approach, Mathematical Biosciences 28 (1976) 25–44.